
TOWARD A NEURO-INSPIRED CREATIVE DECODER

A PREPRINT

Payel Das *

IBM Research, Yorktown Heights, NY, USA
Department of Applied Physics and Applied Math, Columbia University, New York, NY, USA
daspa@us.ibm.com

Brian Quanz *

IBM Research
Yorktown Heights, NY, USA
blquanz@us.ibm.com

Pin-Yu Chen

IBM Research
Yorktown Heights, NY, USA
Pin-Yu.Chen@ibm.com

Jae-wook Ahn

IBM Research
Yorktown Heights, NY, USA
jaewook.ahn@us.ibm.com

May 18, 2022

ABSTRACT

Creativity, a process that generates novel and valuable ideas, involves increased association between task-positive (control) and task-negative (default) networks in brain. Inspired by this seminal finding, in this study we propose a creative decoder that directly modulates the neuronal activation pattern, while sampling from the learned latent space. The proposed approach is fully unsupervised and can be used as off-the-shelf. Our experiments on three different image datasets (MNIST, FMNIST, CELEBA) reveal that the co-activation between task-positive and task-negative neurons during decoding in a deep neural net enables generation of novel artifacts. We further identify sufficient conditions on several novelty metrics towards measuring the creativity of generated samples.

Keywords Machine Learning

1 Introduction

Creativity is often defined as a process that produces ideas that are both novel and valuable. Naturally, the creative process involves a two-fold model that involves idea generation and idea evaluation [1, 2]. The generation phase involves the combination of unfamiliar associations in a novel way, which relies on searches through different forms of memory. The output of generation relies on evaluation that is complementary, and often decisive of the quality or value of the creative product. Nevertheless, it is widely accepted that novelty is a better predictor of creativity than value [3].

How does human brain produce creative ideas? It is an interesting question and has been a central topic in cognitive neuro-science for a long time. Interestingly, a number of recent neuro-imaging studies [4, 5, 6] suggest stronger coupling of default mode network and executive control network in creative brains across a range of creative tasks and domains, from divergent thinking to poetry composition to musical improvisation (see Fig. 1A-B). Brain networks constitute interacting brain regions known to have activity highly correlated with each other and distinct from other networks [7, 8]. Default mode network involves midline posterior and anterior regions, whereas control network includes lateral prefrontal and anterior inferior parietal regions. Default mode network activity is associated with

*Payel Das and Brian Quanz contributed equally to this work and are corresponding authors.

spontaneous and self-generated thought, including mind wandering, mental simulation, social cognition, memory retrieval, and divergent thinking [9, 10, 11]. The control network, on the other hand, is associated with cognitive processes that require externally directed attention, including working memory, relational integration, and task-set switching [9]. The default and control networks often exhibit an antagonistic relation during rest, as well as during many cognitive tasks, including working memory [12]. This antagonistic relation between default and control networks likely reflects suppression of task-unrelated thoughts during cognitive control. In literature, therefore the process of idea evaluation and constraint-directed idea modification is often synonymous to executive control, whereas the idea generation is presumably mediated by default network - in light of its role in self-generated cognition [13, 2]. The dynamic coupling of default and control networks has been previously reported during goal-directed, self-generated thought processes, such as autobiographical future planning [14]. Based on the similar relation between default and control networks observed during creative thinking, it has been proposed that those networks contribute to idea generation and selection, respectively, by means of the evolutionary processes of blind variation and selective retention [13]. A stringent evaluation might hinder creativity in the brain [15] - ideas that are novel but inappropriate are likely to be inhibited and ruled out during evaluation.

Artificial creativity. Since the very early days of computational science, scientists have been exploring artificial agents that can generate creative artifacts or ideas, in areas such as visual art, music, poetry, story, etc. The pioneering work of Margaret Boden clarifies the definition of (computational) creativity, *i.e.* (1) unfamiliar combination of familiar ideas, (2) exploration, and (3) transformation of conceptual spaces, exploratory and transformational considered as higher forms of creativity [16]. Several different approaches have been proposed to guide the search process of an artificial agent in order to make it creative. For example, [17, 18] exploits human-in-the-loop or expert feedback. Out-of-the-box exploration has also been proposed by using the knowledge of reference objects. Along this line, evolutionary algorithms have been used, in which generated samples are improved by using a fitness score in an iterative manner [19, 20, 21]. However, the prerequisite of explicitly defining a fitness function or hard-coded evaluation rules based on the known object description restricts their exploration capability [22].

Recent emergence of data-driven approaches, such as machine learning and especially deep learning models, provide an efficient way of learning from- and reproducing- the training data distribution. In particular, deep generative models like variational autoencoder (VAE) [23, 24] and generative adversarial network (GAN) [25], have received a great deal of attention due to their ability to learn complex, high-dimensional distributions and generate complicated synthetic images. Since these models are designed to be emulative, whether those models can exhibit some form of exploratory creativity is an open question.

1.1 Research Question

This work attempts to induce explorability in a deep generative model by directly modulating the neuronal activation pattern of the generator (see Fig 1C). The proposed approach is motivated by above-mentioned neuro-scientific findings that suggest stronger coupling task-positive and task-negative neurons in creative brains. For this purpose, we introduce creative-VAE, a VAE with a *creative* decoder. A sample is drawn from the learned representation space, as typically obtained by training a VAE model on a set of images. However, during decoding/generation, an atypical activation pattern of the hidden neurons is used to encourage *creative* generation. In this sense, the goal of the original VAE is to learn and generate samples of known types, as accurately as possible. In contrast, our VAE with a *creative* decoder aims to generate novel samples from the original latent (concept) space by favoring co-activation between task-positive and task-negative neurons. We evaluate the novelty and quality of the generated samples using a number of surrogate metrics. We show the performance of the proposed method against MNIST, FMINST, and CELEBA datasets.

Our main contributions are:

- Inspired by findings from functional neuroimaging studies, we propose a VAE model with a *creative* decoder, one that generates novel samples from the learned representation space by atypical coupling of task-positive and task-negative neurons. This modified generation scheme *does not require any data labels* and can be adapted to any decoder/generator.
- Three distinct methods of stochastic co-activation of task-positive and task-negative neurons during decoding are tested: *correlation*, *cluster*, and *default task-negative*.
- The novelty of the generated samples was quantitatively evaluated using a number of surrogate metrics. Our analyses suggest that the sufficient condition to ensure novelty is a combination of low-to-medium classifier entropy, high Frechet inception distance (FID), high distance to the nearest reconstructed sample and large dissimilarity to the training distribution in both input and latent space.

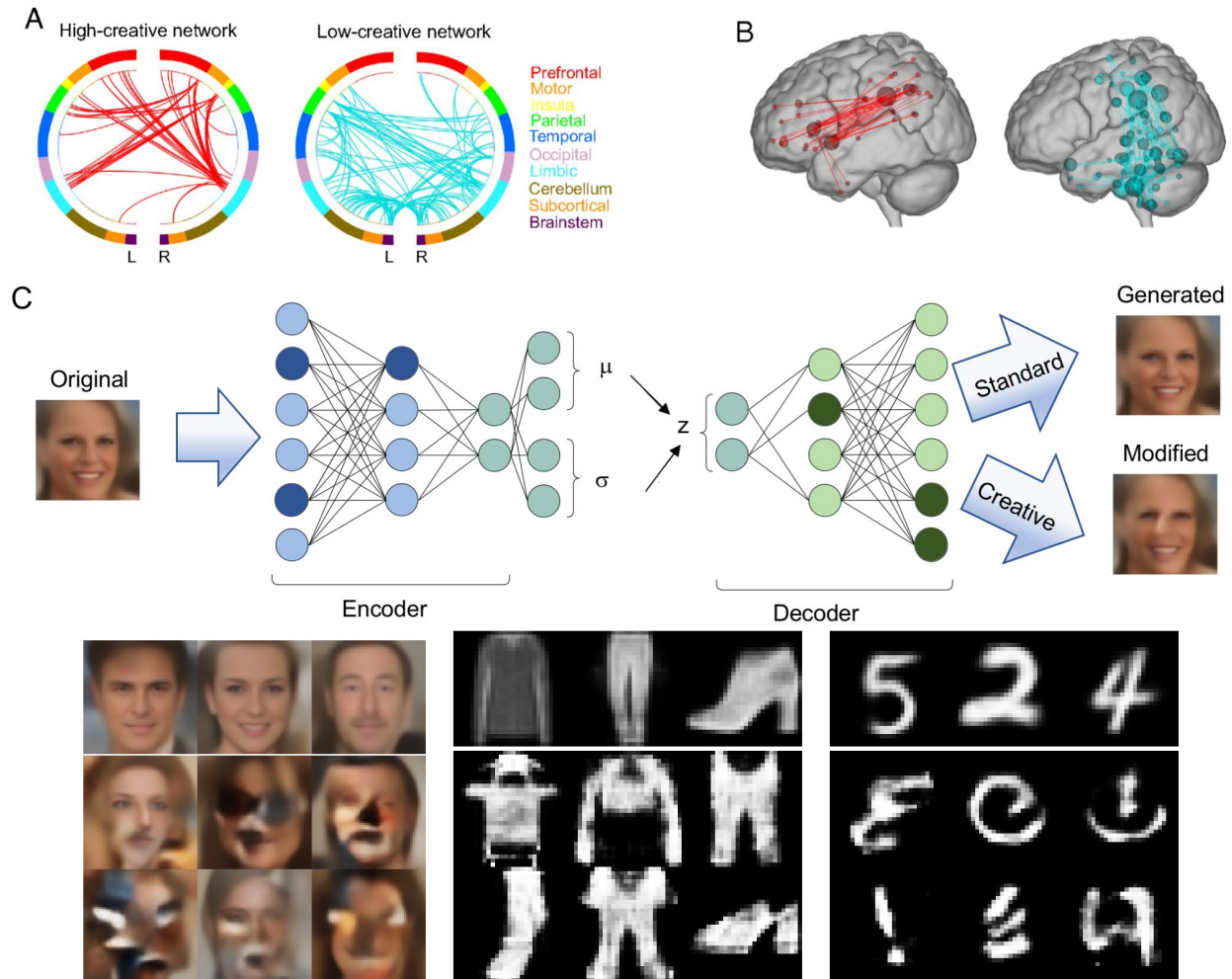


Figure 1: A-B. Depictions of the high- and low-creative networks in human brain. Circle plots (A) and glass brains (B) show the highest degree nodes in the high-creative and low-creative networks. Colors within the circle plots correspond to brain lobes: L, left hemisphere; R, right hemisphere. Adapted from [4]. C. Depiction of a VAE model with the neuro-inspired creative decoder. In normal setting, a small fraction of neurons in each hidden layer remain inactive (colored in dark). Inspired by neuronal modulation observed in creative brains, we activate those “inactive” decoder neurons to induce coupling between task-positive and task-negative neurons during creative generation. **Bottom:** selected creative examples - top row is regular generation; below are creative generation with “default task-negative” method.

- We perform experiments on three different image datasets to illustrate effectiveness of our design. One notable advantage of our method is that it readily applies to any off-the-shelf model as it does not require any retraining, access to abnormal samples, or additional categorical information for creative generation².

2 Related Work

Visual Creativity using Concept Blending Concept blending based on their context and association has been exploited in a number of deep learning models as a form of artificial creativity [16]. The use of multi-layer artificial neural network structure in deep learning models, the design of which was partly inspired by human brain structure, has produced impressive results in visual art generation. Neural pattern blending of two different images using different mathematical formulations has been proposed [26, 27]. Two recent approaches are worth mentioning in this context, Deep Dream

²The codes and data will be made available upon publication.

[28] and Deep Style Transfer [29]. Both Deep Dream and Deep Style Transfer are based on deep convolutional neural networks (CNNs) [30] that are considered to be similar to biological vision blend lower-level, yet abstract, visual features from multiple input images are used to create a new output image. Deep Dream’s working principle is “Whatever you see there, I want more of it!” Therefore, the patterns detected by the CNN from the original input image are repeatedly saturated in successively generated images by a feedback loop, resulting into hallucinating, yet artistic, images. Deep Style Transfer uses neural representations to separate and recombine content and style of arbitrary images, therefore it needs style information to create artistic images. [31] generates new images that are not digit-like by performing operations, like crossover and mutation, in the latent space of MNIST digits learnt by an autoencoder, or by iteratively refining a random input such that it can be easily reconstructed by the trained autoencoder. However, use of a deterministic autoencoder prevents sampling from the latent space, which is possible in deep generative models like VAE [23, 24] and GAN [25]. Visual concept blending has been performed in a number of studies that employ either GAN or VAE [32]. There have been extensions of VAE and GAN that facilitate generating images conditioned on categories/styles [33, 34] or captions [35]. However, those still emulate the original distribution rather than exploring or transforming it. A recent GAN variant termed as creative adversarial network (CAN) has attempted to generate novel artistic images by minimizing deviation from art distribution while maximizing style ambiguity [36]. CAN is based on a psychology based concept that proposes use of style ambiguity as a means to increase arousal potential of an art. However, CAN (and conditional deep generative models) needs data-label pairs as input to generate novel samples that are either style-consistent or style-ambiguous, while our proposed model does not need any label information to generate creative samples.

[37] uses a sequence-to-sequence VAE framework using recurrent neural networks (RNNs) [38] as hypernet, named SketchRNN, to generate creative sketch-drawing. In the SketchRNN work, variability in generated images was explored by varying the temperature parameter during decoding. Therefore, SketchRNN is closest to the present work in spirit, as decoder variability is exploited for creative sample generation in the current model. However, SketchRNN does not vary relationship between neurons in a hidden layer in a neuro-inspired manner while decoding, which is the aim of the present study. The clustered structure of hidden neuron activations arises from the intrinsic redundancy of deep neural network (DNN) parameters and the correlation in input data. Therefore, our aim is to explore, in the spirit of altered neuronal activation pattern observed in creative brain, the effect of co-activating task-positive and task-negative neurons during decoding on the generated samples.

3 Model and Methods

3.1 Variational autoencoder

VAEs [23, 24] aim to model the data likelihood $p(x)$, given samples x from a dataset. Towards this goal, VAE uses a recognition neural network (encoder) and a generative neural network (decoder) to solve the variational inference problem that maximizes the marginalized data likelihood. The trained decoder can then be used to generate synthetic data that looks similar to training data. Nonetheless, the exact data likelihood is frequently intractable, thus VAE approximately maximizes the evidence lower bound (ELBO) by gradient ascent on the objective function: $L(\phi, \theta; x) = E[\log p(z)] + E[\log p(x|z)] - E[\log q(z)] = E[\log p(x|z)] - KL[q(z)||p(z)]$. Therefore, the combined loss function is $L(\phi, \theta; x) = E_{q_\phi(z|x)}[\log p_\theta(x|z)] - KL(q_\phi(z|x)||p(z))$, where θ and ϕ represents parameters of the decoder and encoder, respectively. The first term in the combined loss accounts for the reconstruction loss. The second term measures the KL loss between the distribution of latent codes, $p_\theta(z)$, produced by the encoder, and the prior distribution, typically represented by a diagonal-covariance Gaussian, whose mean and covariance is obtained by passing a noise parameter ϵ through the decoder. Since VAE produces a generative model of the data distribution, novel data points are generated by first sampling $z \sim p(z)$ and then estimating $p_\theta(z)$. On the other hand, the KL regularization enforces the distribution of latent variables to match a prior distribution, so that the generated data has same structure as the training data. As a result, a semantically rich latent z - space is obtained, and simple manipulation, *e.g.* interpolation and arithmetics, in z - space produces meaningful artifacts [37, 39, 40]. Various modified loss objectives [41, 42], complex prior distributions [43, 44] and sophisticated model architectures [45, 46, 47] have been proposed to improve VAE’s performance. In this paper, we solely use the “vanilla” VAE objective with simple Gaussian prior, as described above.

3.2 Creative decoding scheme

To capture the spirit of the atypical neuronal activation pattern observed in a creative human brain, *i.e.* dynamic interaction between a task-positive (control) and a task-negative (default) brain network, we propose a probabilistic decoding scheme. After sampling a given z , it (1) selects decoder neurons based on their activation correlation pattern, and then activates a few “off” neurons along with the typical “on” neurons. Three different co-activation schemes are

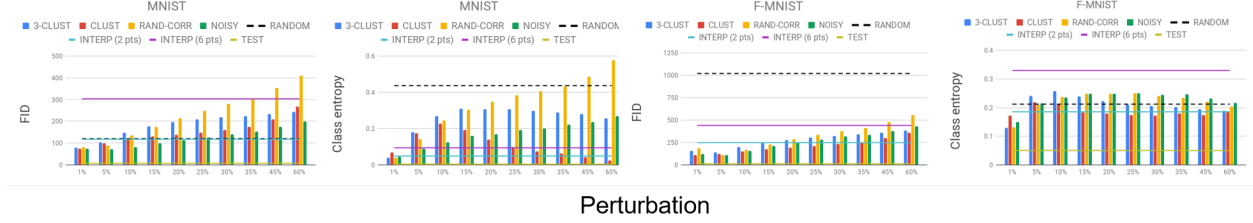


Figure 2: Frechet inception distance (FID) and classifier entropy for MNIST and FMNIST as a function of perturbation (in %).

tested during a specific decoding task: (1) correlation-based – a fraction of neurons that were originally anti-correlated with the firing neurons are turned on; (2) cluster-based – a fraction of neurons chosen from neuron activation cluster(s) that were originally deactivated are activated; and (3) “default task-negative” based – a fraction of neurons that were weakly-activated in the trained decoder across most of the entire training data were turned on.

Preliminaries. Let $d_j^k(z)$ represent the output of the j th neuron of the k th layer given input $z \in \mathcal{Z}$ to the decoder p_θ . We further use the short-hand, $d_{ji}^k = d_j^k(z_i)$, where z_i is the encoding of the i th training data point. Then the *percentage activation* of neuron j in layer k is $a_j^k = (1/n) \sum_{i=1}^n \mathbb{1}_{d_{ji}^k > \tau}$, for a given activation threshold τ . Since we are using RELU activation functions in our experiments we set τ to $1e - 7$. Neurons with $a_j^k \approx 0$ are classified as *dead neurons* and are excluded from modification in each method. Additionally, for the i th input we call neuron j of layer k “active” or “on” if $d_{ji}^k > \tau$, and “inactive” or “off” otherwise. Let \vec{d}_j^k be the vector with i th entry = d_{ji}^k . Given neuron j and neuron h in layer k , let $C^{kjh} = \text{Cov}[\vec{d}_j^k, \vec{d}_h^k]$ (the covariance matrix). Then we define their correlation $R_{jh}^k = C_{01}^{kjh} / \sqrt{C_{00}^{kjh} C_{11}^{kjh}}$ - which are the entries of the layer correlation matrix R^k .

Neuron flipping. We define flipping a neuron “off” by setting it to a minimum activation value, *i.e.*, 0 in the context of RELU activation. We define the “on” value of a neuron j in layer k as $o_j^k = \lambda \cdot s(\{d_{ji}^k | i = 1 \dots n\})$, *i.e.*, as λ denotes a scaling factor for the statistic of training activation values, *e.g.* s equal to mean, max, median, 90th percentile, *etc.* Since, task-negative neurons are activated during creative processes at higher levels than usual (see Introduction), we mainly focus on $s = \text{max}$ and $\lambda = 2$ in these experiments, unless otherwise stated.

We start with a sample $z \sim p(z)$ and obtain the decoder activations for a selected layer k , for which we now use shorthand $d_{jz}^k = d_j^k(z)$. Additionally let \mathcal{A} be the corresponding set of active or “on” neurons and \mathcal{D} the set of inactive or “off” neurons. During creative decoding, we flip some percentage, ρ , of a group of “on” and/or “off” neurons in a layer k , either randomly or selectively. Each method, as described next, modifies $d_{jz}^k(z)$, and this modified layer output is then passed through the remainder of the decoder, to obtain the final generated values.

Correlation method. The correlation method first (1) randomly selects a neuron from the \mathcal{D} group that is least-correlated with the most-activated group of neurons; then (2) selects additional neurons that are correlated with the selected deactivated neuron; and (3) finally turns all of them on. The idea is that, these deactivated neurons are not correlated with the most active ones, and so can be viewed as instance-specific task-negative neurons. By using correlation, concepts encoded in multiple neurons can possibly be better captured than pure random selection. Optionally, the same number of neurons can be turned off from those most correlated with the selected high-active neurons. Details is provided in Algorithm 1.

Algorithm 1 Correlation method

Input: Layer output d_{jz}^k ; selection fraction κ ; fraction of neurons to flip on ρ

$$\begin{aligned} \gamma_j &\leftarrow (1/|\mathcal{A}|) \sum_{h \in \mathcal{A}} R_{jh}^k d_{hz}^k, j \in \mathcal{D} \\ s &\leftarrow \text{random select from smallest } \kappa|\mathcal{D}| \text{ neurons of } \{\gamma_j\} \\ \mathcal{D}_s &\leftarrow \text{argmax}_{\mathcal{D}' \subset \mathcal{D}, |\mathcal{D}'| = \lfloor \rho|\mathcal{A}| \rfloor} \sum_{h \in \mathcal{D}'} R_{sh}^k \\ d_{jz}^k &\leftarrow o_j^k, \forall j \in \mathcal{D}_s \end{aligned}$$

Clustering method. The clustering method follows a similar approach as the correlation method, except instead of considering individual neurons, clusters of neurons are considered, which represent instance-specific task-negative sub-networks. Spectral clustering [48] is applied to the layer output correlation matrices from the training data (R^k) to

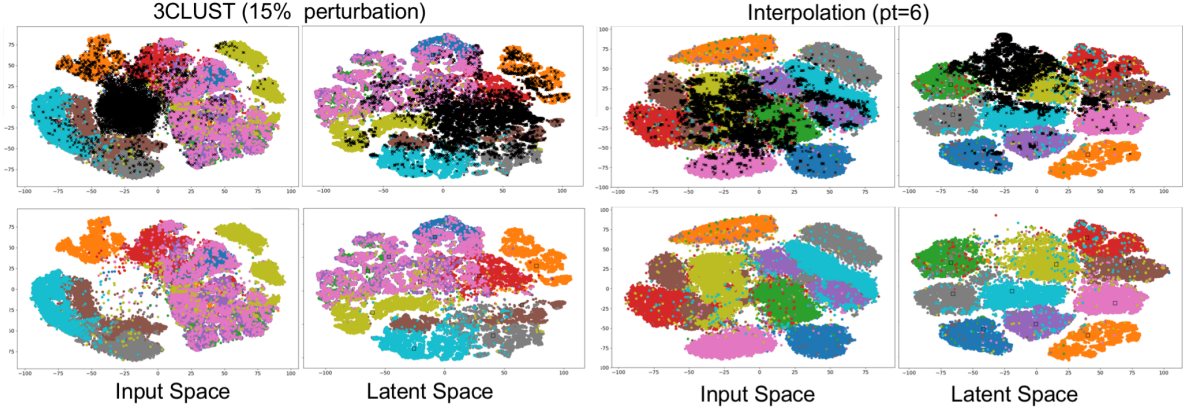


Figure 3: 2D projection, as obtained by performing t-SNE[49] on an FMNIST ensemble of generated samples and training images. Black dots represent creative samples, while each of the remaining colors denotes a specific FMNIST class.

get the cluster memberships. For a given instance and decoder layer, one-or-more clusters with lowest percent activation are randomly selected, where percent activation for cluster \mathcal{C}^k is $(1/|\mathcal{C}^k|) \sum_{j \in \mathcal{C}^k} \mathbb{1}_{d_{jz}^k > \tau}$. The percent activations of the selected clusters are then increased by randomly turning on more neurons in those clusters until the specified percent increase is reached.

“Default task-negative” method. The “Default task-negative” method (Algorithm 2) captures the task-negative concept in a more realistic sense - by identifying those neurons that typically have low activation across all the training data and turning some fraction of them on at test time. Specifically, a neuron is selected from deactivated neurons that have the lowest percent activations (a_j^k). Next, “default task-negative” neurons that are strongly correlated with the selected neuron are turned on.

Algorithm 2 Low-active method

Input: Layer output d_{jz}^k ; percent activation percentile κ ; fraction of neurons to flip on ρ

$$t \leftarrow \kappa\text{-percentile}(\{a_j^k\})$$

$$\mathcal{S} \leftarrow \{j | j \in \mathcal{D} \wedge a_j^k \leq t\}$$

$$s \leftarrow \text{random select from } \mathcal{S}$$

$$\mathcal{S}_s \leftarrow \text{argmax}_{\mathcal{S}' \subset \mathcal{S}, |\mathcal{S}'| = \lfloor \rho |\mathcal{S}| \rfloor} \sum_{h \in \mathcal{S}'} R_{sh}^k$$

$$d_{jz}^k \leftarrow o_j^k, \forall j \in \mathcal{S}_s$$

3.3 Experimental Details

VAE architecture and hyperparameters. For F/MNIST the encoder network consisted of 3 fully-connected layers, and for CelebA, consisted of 9 convolutional layers. The decoder reverse architecture of the corresponding encoder. RELU activations were used; dropout [50] equals to 0.10 for fully-connected layers. z dimension size was set to 50 for F/MNIST and 128 for CelebA.

Classifier. The classifiers consisted of 5 convolutional layers with RELU and dropout = 0.10, yielding test accuracy of 99.28% for MNIST and 92.99% for FMNIST. For details on VAE and classifier architecture, see Supplementary Material.

Creative decoding. The samples generated by the creative decoding scheme were compared with the original distributions as well as with samples generated by (1) INTERP: linear interpolation in the latent space between a number of training samples (points) that belong to different class, followed by standard decoding, (2) NOISY: random sampling from the latent space, followed by noisy decoding, during which a random Gaussian noise was infused in a fraction of neurons in the 3rd hidden layer, and (3) RANDOM: creating random images from multivariate Gaussian, whose mean and variance were estimated from the original dataset. We performed modifications at the 3rd hidden layer of the decoder, since some amount of transformation from the z -space should be necessary to capture the underlying

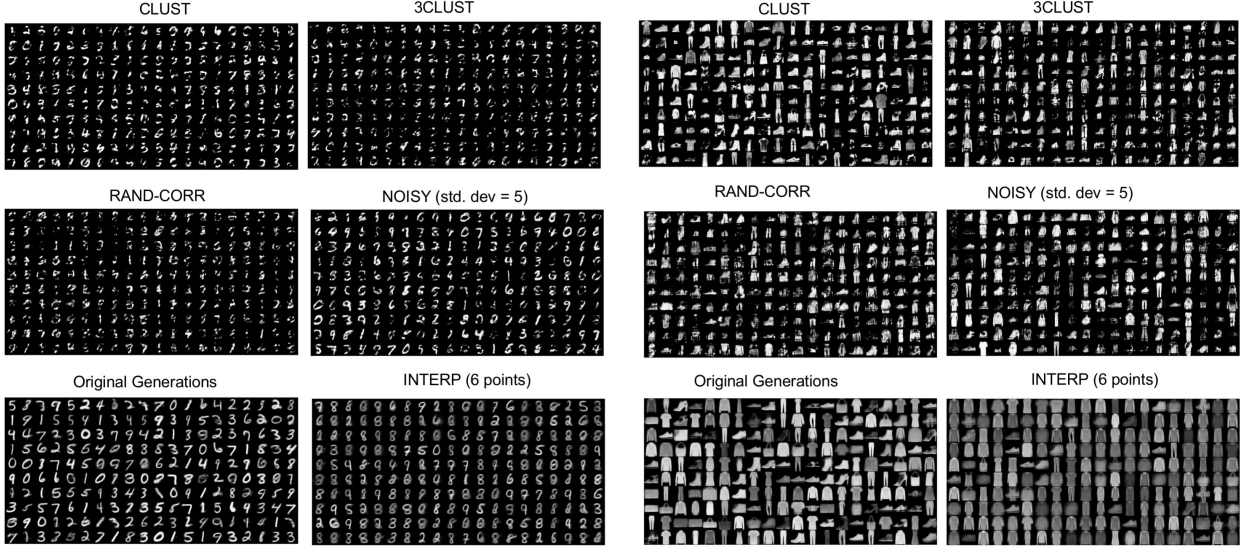


Figure 4: Samples of generated MNIST and FMNIST images. 15% perturbation was used for both creative decoder and noisy decoder.

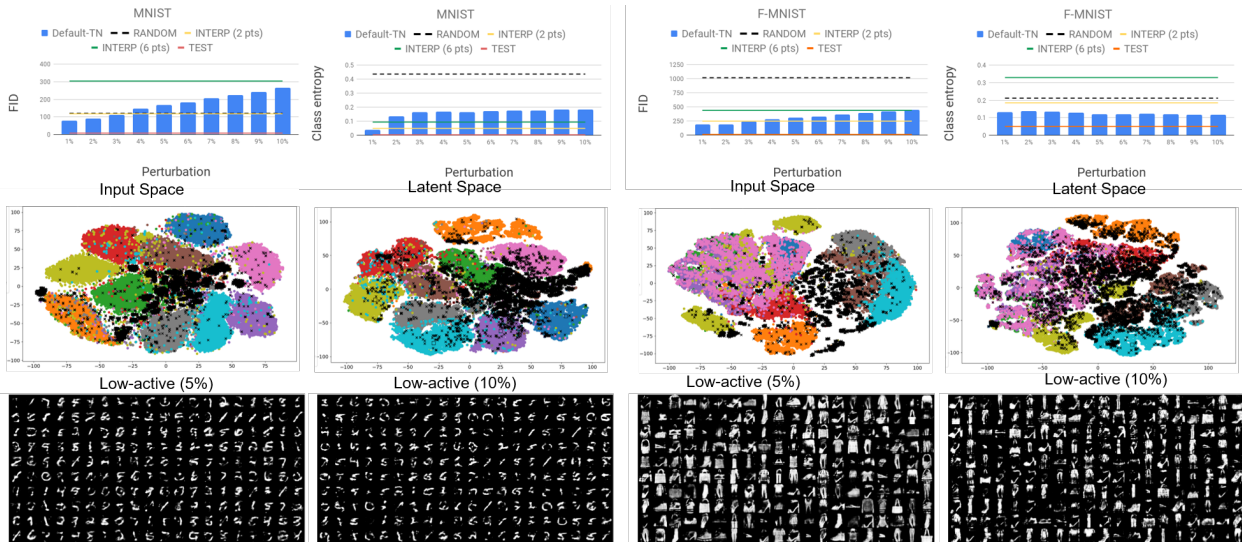


Figure 5: FID, entropy, t-SNE embeddings and MNIST/FMNIST images generated by co-activating “default task-negative” neurons.

data invariances and structure that is then decoded to the final image. However, modifying lower layers also produced variety of creative results - full analyses of how decoder layer choice impacts results is left for future work.

3.4 Novelty Metrics

Due to an expanding volume of research in deep generative models in last few years, several new methods for novelty detection have been proposed. The novelty evaluation of generated samples in a quantitative manner is tricky, given the original generative model has access to training samples only. Previous studies have used likelihood [51], or a combination of reconstruction error and likelihood [52] for this purpose. Nevertheless, the likelihood estimation is frequently intractable and inadequate [53, 54]. Therefore, reconstruction error alone [55, 56], reconstruction probability [57], and a combination of combination of reconstruction error and likelihood [52] have been proposed. Alternatively, density and distance-based approaches have been used [55, 56, 58]. In the present study, we evaluate

Table 1: $k - NS$ (in input and latent space) and D_{recon} .

		15%					35%				
		1-NS _d	5-NS _d	1-NS _z	5-NS _z	D _{recon}	1-NS _d	5-NS _d	1-NS _z	5-NS _z	D _{recon}
MNIST	TEST	1.096	1.079	1.079	1.048	3.652					
	RAND-CORR	1.633	1.529	1.354	1.251	4.744	1.911	1.794	1.583	1.406	4.728
	CLUST	1.534	1.441	1.325	1.225	4.924	1.446	1.364	1.272	1.184	4.667
	3CLUST	1.643	1.534	1.378	1.268	4.946	1.718	1.607	1.505	1.352	4.968
	NOISY	1.355	1.283	1.241	1.165	3.029	1.534	1.447	1.367	1.256	3.626
	INTERP	2 pts					6 pts				
		1.001	0.964	1.116	1.068	1.477	1.029	0.982	1.108	1.056	1.586
Default TN	5%					10%					
	1.476	1.38	1.301	1.206	4.988	1.553	1.439	1.402	1.274	5.191	
FMNIST	TEST	1.192	1.155	1.071	1.031	3.430					
	RAND-CORR	1.581	1.506	1.505	1.325	5.387	1.568	1.508	1.679	1.449	5.420
	CLUST	1.499	1.405	1.429	1.277	5.006	1.545	1.444	1.424	1.281	5.160
	3CLUST	1.576	1.495	1.549	1.351	5.500	1.572	1.507	1.567	1.382	5.702
	NOISY	1.454	1.394	1.52	1.327	3.809	1.462	1.415	1.612	1.409	4.491
	INTERP	2 pts					6 pts				
		0.966	0.933	1.089	1.046	1.210	0.976	0.938	1.086	1.045	1.360
Default TN	5%					10%					
	1.653	1.551	1.409	1.257	5.547	1.657	1.567	1.462	1.288	5.808	
CELEBA	TEST	1.774	1.785	1.516	1.332	9.346					
	Default TN	5%					10%				
		2.397	2.316	1.800	1.709	13.537	3.008	2.896	1.885	1.822	16.590

novelty with respect to four different metrics, classifier entropy, Fréchet Inception Distance (FID), reconstruction distance, and local neighborhood based k-novelty score.

Entropy. Entropy of the probabilities p returned by a trained, multi-class classifier can be used to estimate novelty of generated samples [59, 60], which can be defined as $E = -\sum_i p_i \log_2 p_i$. A higher value of E implies higher novelty.

Fréchet Inception Distance. The FID [61] provides an alternative approach that requires no labeled data. The samples are first embedded in some feature space (a specific layer) of a trained classifier and a continuous multivariate Gaussian is fit to the embedding layer. Then, mean and covariance is estimated for both the generated and training data. The Fréchet distance between these two Gaussians is then computed as the Fréchet Inception Distance or $FID(x, g) = \|\mu_x - \mu_g\|_2^2 + Tr(\sum_x + \sum_g 2(\sum_x \sum_g)^{\frac{1}{2}})$, where (μ_x, \sum_x) , and (μ_g, \sum_g) are the mean and covariance of the sample embeddings from the data distribution and model distribution, respectively. Lower FID means smaller distances between synthetic and real distributions. FID is found to be sensitive to addition of spurious modes, to mode dropping, and is consistent with human judgment, while may not capture “memory overfitting” [62].

Distance to the nearest re-generated sample. For a given image x and corresponding latent vector z , novelty can be estimated in terms of the distance, between x and the closest sample the VAE can produce from z . Therefore, $D_{recon} = \min_z \|x - E_{\theta}(x|z)\|_2$. Since a trained VAE has a narrow bottleneck, the reconstruction of any novel image will be far apart from it.

k-Novelty score. We estimate the nearest-neighbors distance between a generated sample and the training dataset in the latent z space and in input space. We use normalized k -NN distance as a novelty score [63]. The kNN novelty score (k -NS) of a given data point is the distance to its k th nearest neighbor, denoted as $kNN(\cdot)$, in the training dataset, normalized by k -NN distance between the $kNN(\cdot)$ and its k nearest neighbors. Therefore, $k-NS = \frac{d(x, kNN(x))}{d(kNN(x), kNN(kNN(x)))}$. For $k = 1$, d is an l_2 distance. For $k > 1$, d accounts for the average distance to the k nearest neighbors. We estimate k -NN for $k=1$ and 5.

3.5 Novelty evaluation

The classifier entropy and FID of the generated samples using different decoding scheme (creative and noisy decoder) are shown in Fig. 2. The values for test, RANDOM and INTERP samples are also shown for comparison. With increasing % perturbation, entropy increases to a maximum, and then decreases, except for the RAND-CORR decoding on MNIST. At low perturbations, 3CLUST results in highest entropy, while RAND-CORR outperforms at higher values of perturbation. Co-activation of a single cluster (CLUST) always yields lower entropy compared to 3CLUST and RAND-CORR. Noisy decoder yields similar performance as RAND-CORR on FMNIST, although entropy on MNIST

generations is significantly smaller. The FID trend, as shown in Fig. 2), clearly shows that, for both MNIST and FMNIST, 3CLUST yields higher FID up to 15% perturbations, while at larger perturbations RAND-CORR outperforms. Again, co-activation of a single deactivated cluster performs weaker than 3CLUST. FID for noisy decoder is consistently small for both dataset, particularly for lower range of perturbation. In summary, 3CLUST yields higher or competitive FID and entropy at smaller perturbations, whereas RAND-CORR performs better at higher values. For practicality issues, it makes sense to induce creativity in a trained generative model like the one used in this study by only perturbing it minimally (low-cost perturbation). Our results suggest that, subtle neuronal perturbation that accounts for the intrinsic structure of a trained neural net is capable of generating a distribution with high diversity as well as high entropy.

This trend is also evident from the k - NS and D_{recon} values (Table 1). Again, while both creative decoder and noisy decoder yields high novelty score with respect to the test images. At low (15%) perturbation, 3-CLUST decoding of MNIST results in highest novelty score and reconstruction distance in both latent and input space. For FMNIST, 3-CLUST samples outperform in terms of novelty score in latent space and D_{recon} , while RAND-CORR samples show highest novelty in input space. Interestingly, the interpolated ones consistently yield low k - NS even compared to the test samples, indicating that simple interpolation in the latent space does not result in novel samples. These results are consistent with the t-SNE embeddings of the input and latent space computed on a dataset comprised of training and generated images (see Fig. 3). The 3-CLUST samples form a distinct cluster of their own in the input space, separated from the training data. Those novel images also occupy sparsely-populated regions in the latent space. In contrast, the not-so-novel INTERP samples appear highly similar to the original images in the pixel space, although those also fill up some underpopulated regions in the z space. It is likely that the trained VAE has a narrow bottleneck (as the trained model cannot generate any random/abnormal data) due to the KL regularization term, and therefore, the novel images as well as the ones obtained using interpolation are mapped to different regions of the latent space. The ones generate by creative decoding are clearly more novel, compared to both NOISY and INTERP, as evident from the examples shown in Fig. 4. More examples of t-SNE embeddings and generated images can be found in Supplementary Material. These findings suggest that sufficient conditions to measure creativity of generated samples should include several unsupervised metrics that include information of both input and latent space.

3.6 Creative generation in the “default” mode

These results motivate us to design further control over creative decoder, again inspired by findings from functional brain imaging, that the default (task-negative) network in brain has shown an antagonistic relationship with control (task-positive) network. Therefore, we define a “default” mode in the decoder (in an over-simplified manner), by identifying the hidden neurons that show consistently low activation ($< 15\%$) across the entire training distribution; we refer to those neurons as *default task-negative or default TN*. A small fraction ($< 10\%$) of those default TN neurons that were deactivated during original decoding are “turned on” by the creative decoder. The results are shown in Table 1 and in Fig. 5. While the entropy is slightly compromised, FID, D_{recon} , and k - NS values are comparable or better than 3CLUST, CLUST, RAND-CORR, and NOISY decoders. It is impressive that such a subtle neuronal modulation, in which only $\leq 0.01\%$ neurons are perturbed, yields in creative generation. While those images are still visually recognizable as digits and fashion categories, they appear more novel and diverse, compared to those shown in Fig. 4, consistent with higher novelty metrics.

3.6.1 CelebA Results

We also evaluate the performance of our creative decoder on the more complex CelebA dataset. Table 1 reports D_{recon} and k - NS for CelebA test images as well as the ones generated by default-TN method. Again, the results suggest higher novelty score and reconstruction distance with respect to the test images, implying that our method generates creative artifacts across a variety of datasets. CelebA examples generated by default-TN decoder are shown in Fig 6. Notably, many of those underwent an asymmetric modification (darkening/fading) near the eyes.

4 Discussion and Future work

Prior work has shown that high decoder capacity enables easier posterior inference; at the same time the model becomes prone to over-fitting [39, 64, 65]. In fact, high capacity decoders in a VAE-setting are known to ignore latent information while generating, which has been widely addressed recently. A number of solutions have been proposed, from “KL cost annealing” [39] to use of a “free bits” constraint on the minimum value of the KL term [64] to the use of flexible variational distributions [43, 44]. Methods like InfoGAN [46] and β -VAE [42] have been further proposed that are capable of learning disentangled and interpretable representations in an unsupervised fashion by enforcing a stronger constraint on the latent bottleneck.



Figure 6: CelebA images obtained by activating default TN neurons.

The presence of inactive latent units in a trained VAE model originates from regularization or network pruning. The present study shows that, this extra *unused* capacity can be exploited to induce creativity during generation. In a sense, the proposed method functions in the opposite direction of denoising autoencoders [66] and sparse autoencoders [67]. While our aim is not to downplay the complexity of the human brain and the creative cognition process, the fact that exploiting the extra unused capacity in a trained decoder provides access to novel images in a brain-inspired fashion is interesting and demands further investigation. Towards that goal, future work will include trainable decoder that enforces creativity by purposefully adding extra capacity and exposing the model to a more complicated multi-task setting. It will be also interesting to investigate memory retrieval in a deep neural net by disentangling those “default task-negative” neurons and then activating them at test time.

References

- [1] Ronald A Finke, Thomas B Ward, and Steven M Smith. Creative cognition: Theory, research, and applications. 1992.
- [2] Oded M Kleinmintz, Tal Ivancovsky, and Simone G Shamay-Tsoory. The twofold model of creativity: the neural underpinnings of the generation and evaluation of creative ideas. *Current Opinion in Behavioral Sciences*, 27:131–138, 2019.
- [3] Jennifer Diedrich, Mathias Benedek, Emanuel Jauk, and Aljoscha C Neubauer. Are creative ideas novel and useful? *Psychology of Aesthetics, Creativity, and the Arts*, 9(1):35, 2015.
- [4] Roger E Beaty, Yoed N Kenett, Alexander P Christensen, Monica D Rosenberg, Mathias Benedek, Qunlin Chen, Andreas Fink, Jiang Qiu, Thomas R Kwapil, Michael J Kane, et al. Robust prediction of individual creative ability from brain functional connectivity. *Proceedings of the National Academy of Sciences*, page 201713532, 2018.
- [5] Liang Shi, Jiangzhou Sun, Yunman Xia, Zhiting Ren, Qunlin Chen, Dongtao Wei, Wenjing Yang, and Jiang Qiu. Large-scale brain network connectivity underlying creativity in resting-state and task fmri: cooperation between default network and frontal-parietal network. *Biological psychology*, 135:102–111, 2018.
- [6] Zhenni Gao, Delong Zhang, Aiyang Liang, Bishan Liang, Zengjian Wang, Yuxuan Cai, Junchao Li, Mengxia Gao, Xiaojin Liu, Song Chang, et al. Exploring the associations between intrinsic brain connectivity and creative ability using functional connectivity strength and connectome analysis. *Brain connectivity*, 7(9):590–601, 2017.

- [7] Michael D Greicius, Ben Krasnow, Allan L Reiss, and Vinod Menon. Functional connectivity in the resting brain: a network analysis of the default mode hypothesis. *Proceedings of the National Academy of Sciences*, 100(1):253–258, 2003.
- [8] Michael D Fox, Abraham Z Snyder, Justin L Vincent, Maurizio Corbetta, David C Van Essen, and Marcus E Raichle. The human brain is intrinsically organized into dynamic, anticorrelated functional networks. *Proceedings of the National Academy of Sciences*, 102(27):9673–9678, 2005.
- [9] Steven L Bressler and Vinod Menon. Large-scale brain networks in cognition: emerging methods and principles. *Trends in cognitive sciences*, 14(6):277–290, 2010.
- [10] Naama Mayseless, Ayelet Eran, and Simone G Shamay-Tsoory. Generating original ideas: The neural underpinning of originality. *Neuroimage*, 116:232–239, 2015.
- [11] Kalina Christoff, Zachary C Irving, Kieran CR Fox, R Nathan Spreng, and Jessica R Andrews-Hanna. Mind-wandering as spontaneous thought: a dynamic framework. *Nature Reviews Neuroscience*, 17(11):718, 2016.
- [12] Alan Anticevic, Michael W Cole, John D Murray, Philip R Corlett, Xiao-Jing Wang, and John H Krystal. The role of default network deactivation in cognition and disease. *Trends in cognitive sciences*, 16(12):584–592, 2012.
- [13] Roger E Beaty, Mathias Benedek, Paul J Silvia, and Daniel L Schacter. Creative cognition and brain network dynamics. *Trends in cognitive sciences*, 20(2):87–95, 2016.
- [14] R Nathan Spreng, Kathy D Gerlach, Gary R Turner, and Daniel L Schacter. Autobiographical planning and the brain: activation and its modulation by qualitative features. *Journal of cognitive neuroscience*, 27(11):2147–2157, 2015.
- [15] Roger E Beaty, Alexander P Christensen, Mathias Benedek, Paul J Silvia, and Daniel L Schacter. Creative constraints: Brain activity and network dynamics underlying semantic interference during idea production. *Neuroimage*, 148:189–196, 2017.
- [16] Margaret A Boden. *The creative mind: Myths and mechanisms*. Routledge, 2004.
- [17] Jeanine Graf and Wolfgang Banzhaf. Interactive evolution of images. In *Evolutionary Programming*, pages 53–65, 1995.
- [18] Akin Osman Kazakci. Conceptive artificial intelligence: Insights from design theory. *arXiv preprint arXiv:1404.0640*, 2014.
- [19] Steve DiPaola and Liane Gabora. Incorporating characteristics of human creativity into an evolutionary art algorithm. *Genetic Programming and Evolvable Machines*, 10(2):97–110, 2009.
- [20] Penousal Machado, Juan Romero, and Bill Manaris. Experiments in computational aesthetics. In *The art of artificial evolution*, pages 381–415. Springer, 2008.
- [21] Hideyuki Takagi. Interactive evolutionary computation: Fusion of the capabilities of ec optimization and human evaluation. *Proceedings of the IEEE*, 89(9):1275–1296, 2001.
- [22] J Parikka. Leonardo book review: The art of artificial evolution: A handbook on evolutionary art and music, 2008.
- [23] Diederik P Kingma and Max Welling. Auto-encoding variational bayes. *arXiv preprint arXiv:1312.6114*, 2013.
- [24] Danilo Jimenez Rezende, Shakir Mohamed, and Daan Wierstra. Stochastic backpropagation and approximate inference in deep generative models. *arXiv preprint arXiv:1401.4082*, 2014.
- [25] Ian Goodfellow, Jean Pouget-Abadie, Mehdi Mirza, Bing Xu, David Warde-Farley, Sherjil Ozair, Aaron Courville, and Yoshua Bengio. Generative adversarial nets. In *Advances in neural information processing systems*, pages 2672–2680, 2014.
- [26] Paul Thagard and Terrence C Stewart. The aha! experience: Creativity through emergent binding in neural networks. *Cognitive science*, 35(1):1–33, 2011.
- [27] Diederik Aerts, Jan Broekaert, Liane Gabora, and Sandro Sozzo. Generalizing prototype theory: A formal quantum framework. *Frontiers in psychology*, 7:418, 2016.
- [28] Christian Szegedy, Wei Liu, Yangqing Jia, Pierre Sermanet, Scott Reed, Dragomir Anguelov, Dumitru Erhan, Vincent Vanhoucke, and Andrew Rabinovich. Going deeper with convolutions. In *Proceedings of the IEEE conference on computer vision and pattern recognition*, pages 1–9, 2015.
- [29] Leon A Gatys, Alexander S Ecker, and Matthias Bethge. A neural algorithm of artistic style. *arXiv preprint arXiv:1508.06576*, 2015.
- [30] Alex Krizhevsky, Ilya Sutskever, and Geoffrey E Hinton. Imagenet classification with deep convolutional neural networks. In *Advances in neural information processing systems*, pages 1097–1105, 2012.

- [31] Akin Kazakçian and Mehdi Cherti and Balázs Kégl. Digits that are not: Generating new types through deep neural nets. *arXiv preprint arXiv:1606.04345*, 2016.
- [32] Joel Simon. Ganbreeder: A new way to create and share images g. 2018.
- [33] Wei Ren Tan, Chee Seng Chan, Hernán E Aguirre, and Kiyoshi Tanaka. Artgan: Artwork synthesis with conditional categorical gans. In *Image Processing (ICIP), 2017 IEEE International Conference on*, pages 3760–3764. IEEE, 2017.
- [34] Xinchun Yan, Jimei Yang, Kihyuk Sohn, and Honglak Lee. Attribute2image: Conditional image generation from visual attributes. In *European Conference on Computer Vision*, pages 776–791. Springer, 2016.
- [35] Scott Reed, Zeynep Akata, Xinchun Yan, Lajanugen Logeswaran, Bernt Schiele, and Honglak Lee. Generative adversarial text to image synthesis. *arXiv preprint arXiv:1605.05396*, 2016.
- [36] Ahmed Elgammal, Bingchen Liu, Mohamed Elhoseiny, and Marian Mazzone. Can: Creative adversarial networks, generating "art" by learning about styles and deviating from style norms. *arXiv preprint arXiv:1706.07068*, 2017.
- [37] David Ha and Douglas Eck. A neural representation of sketch drawings. *arXiv preprint arXiv:1704.03477*, 2017.
- [38] Sepp Hochreiter and Jürgen Schmidhuber. Long short-term memory. *Neural computation*, 9(8):1735–1780, 1997.
- [39] Samuel R Bowman, Luke Vilnis, Oriol Vinyals, Andrew M Dai, Rafal Jozefowicz, and Samy Bengio. Generating sentences from a continuous space. *arXiv preprint arXiv:1511.06349*, 2015.
- [40] Adam Roberts, Jesse Engel, and Douglas Eck. Hierarchical variational autoencoders for music. In *NIPS Workshop on Machine Learning for Creativity and Design*, 2017.
- [41] Shengjia Zhao, Jiaming Song, and Stefano Ermon. Infovae: Information maximizing variational autoencoders. *arXiv preprint arXiv:1706.02262*, 2017.
- [42] Irina Higgins, Loic Matthey, Arka Pal, Christopher Burgess, Xavier Glorot, Matthew Botvinick, Shakir Mohamed, and Alexander Lerchner. beta-vae: Learning basic visual concepts with a constrained variational framework. 2016.
- [43] Danilo Jimenez Rezende and Shakir Mohamed. Variational inference with normalizing flows. *arXiv preprint arXiv:1505.05770*, 2015.
- [44] Tim R Davidson, Luca Falorsi, Nicola De Cao, Thomas Kipf, and Jakub M Tomczak. Hyperspherical variational auto-encoders. *arXiv preprint arXiv:1804.00891*, 2018.
- [45] Casper Kaae Sønderby, Tapani Raiko, Lars Maaløe, Søren Kaae Sønderby, and Ole Winther. Ladder variational autoencoders. In *Advances in neural information processing systems*, pages 3738–3746, 2016.
- [46] Xi Chen, Diederik P Kingma, Tim Salimans, Yan Duan, Prafulla Dhariwal, John Schulman, Ilya Sutskever, and Pieter Abbeel. Variational lossy autoencoder. *arXiv preprint arXiv:1611.02731*, 2016.
- [47] Ishaan Gulrajani, Kundan Kumar, Faruk Ahmed, Adrien Ali Taiga, Francesco Visin, David Vazquez, and Aaron Courville. Pixelvae: A latent variable model for natural images. *arXiv preprint arXiv:1611.05013*, 2016.
- [48] Ulrike Von Luxburg. A tutorial on spectral clustering, 2007.
- [49] Laurens van der Maaten and Geoffrey Hinton. Visualizing data using t-sne. *Journal of machine learning research*, 9(Nov):2579–2605, 2008.
- [50] Nitish Srivastava, Geoffrey Hinton, Alex Krizhevsky, Ilya Sutskever, and Ruslan Salakhutdinov. Dropout: a simple way to prevent neural networks from overfitting. *The Journal of Machine Learning Research*, 15(1):1929–1958, 2014.
- [51] Valentin Leveau and Alexis Joly. Adversarial autoencoders for novelty detection. 2017.
- [52] Bo Zong, Qi Song, Martin Renqiang Min, Wei Cheng, Cristian Lumezanu, Daeki Cho, and Haifeng Chen. Deep autoencoding gaussian mixture model for unsupervised anomaly detection. 2018.
- [53] Yuhuai Wu, Yuri Burda, Ruslan Salakhutdinov, and Roger Grosse. On the quantitative analysis of decoder-based generative models. *arXiv preprint arXiv:1611.04273*, 2016.
- [54] Lucas Theis, Aäron van den Oord, and Matthias Bethge. A note on the evaluation of generative models. *arXiv preprint arXiv:1511.01844*, 2015.
- [55] Thomas Schlegl, Philipp Seeböck, Sebastian M Waldstein, Ursula Schmidt-Erfurth, and Georg Langs. Unsupervised anomaly detection with generative adversarial networks to guide marker discovery. In *International Conference on Information Processing in Medical Imaging*, pages 146–157. Springer, 2017.
- [56] Huan-gang Wang, Xin Li, and Tao Zhang. Generative adversarial network based novelty detection using minimized reconstruction error. *Frontiers of Information Technology & Electronic Engineering*, 19(1):116–125, 2018.

- [57] Jinwon An and Sungzoon Cho. Variational autoencoder based anomaly detection using reconstruction probability. *Special Lecture on IE*, 2:1–18, 2015.
- [58] Aleksei Vasilev, Vladimir Golkov, Ilona Lipp, Eleonora Sgarlata, Valentina Tomassini, Derek K Jones, and Daniel Cremers. q-space novelty detection with variational autoencoders. *arXiv preprint arXiv:1806.02997*, 2018.
- [59] Dan Hendrycks and Kevin Gimpel. A baseline for detecting misclassified and out-of-distribution examples in neural networks. *arXiv preprint arXiv:1610.02136*, 2016.
- [60] Mark Kliger and Shachar Fleishman. Novelty detection with gan. *arXiv preprint arXiv:1802.10560*, 2018.
- [61] Martin Heusel, Hubert Ramsauer, Thomas Unterthiner, Bernhard Nessler, and Sepp Hochreiter. Gans trained by a two time-scale update rule converge to a local nash equilibrium. In *Advances in Neural Information Processing Systems*, pages 6626–6637, 2017.
- [62] Mario Lucic, Karol Kurach, Marcin Michalski, Sylvain Gelly, and Olivier Bousquet. Are gans created equal? a large-scale study. In *Advances in neural information processing systems*, pages 698–707, 2018.
- [63] Xuemei Ding, Yuhua Li, Ammar Belatreche, and Liam P Maguire. An experimental evaluation of novelty detection methods. *Neurocomputing*, 135:313–327, 2014.
- [64] Durk P Kingma, Tim Salimans, Rafal Jozefowicz, Xi Chen, Ilya Sutskever, and Max Welling. Improved variational inference with inverse autoregressive flow. In *Advances in neural information processing systems*, pages 4743–4751, 2016.
- [65] Chris Cremer, Xuechen Li, and David Duvenaud. Inference suboptimality in variational autoencoders. *arXiv preprint arXiv:1801.03558*, 2018.
- [66] Pascal Vincent, Hugo Larochelle, Isabelle Lajoie, Yoshua Bengio, and Pierre-Antoine Manzagol. Stacked denoising autoencoders: Learning useful representations in a deep network with a local denoising criterion. *Journal of machine learning research*, 11(Dec):3371–3408, 2010.
- [67] Alireza Makhzani and Brendan Frey. K-sparse autoencoders. *arXiv preprint arXiv:1312.5663*, 2013.
- [68] Diederik P Kingma and Jimmy Ba. Adam: A method for stochastic optimization. *arXiv preprint arXiv:1412.6980*, 2014.

Supplementary Material

Datasets

Three datasets were considered in this study: MNIST, a database of hand-written digits, and FMNIST, a database of fashion categories, both contain 60000 training and 10000 test images, each image is 28×28 pixel grayscale and associated with a label from one of the 10 classes. CelebA is a database of 200,000 aligned and cropped 178×218 -pixel RGB images of celebrity faces, re-sized to 64×64 (200599 training and 2000 test).

Model and Methods

For F/MNIST the encoder network consisted of 3 fully-connected layers (1000, 500, 250), and for CelebA, 9 convolutional layers (3 groups with 32, 64, then 128 filters - each having $2 \times 3 \times 3$ kernels then $1 \times 2 \times 2$, with strides 2, 2, and 1) followed by 2 fully-connected layers (1000, 500). RELU activations were used in addition to a dropout probability [50] of 0.10 for fully-connected layers. The latent dimension size was set to 50 for F/MNIST and 128 for CelebA. The decoder architecture is the reverse of the corresponding encoder (deconvolution for convolution). All VAE experiments were performed with ADAM optimization [68] using a batch size of 128, 200-400 epochs with best validation score model kept and re-starts from best used. Test loss (KL and reconstruction) was 10.8 and 230.8 for FMNIST, 13.7 and 96.3 for MNIST, and 577.7 and 75259.5 for CelebA (for CelebA means-squared error was used for the reconstruction loss and scaled by $1e7$).

Classifier

The classifiers consisted of 5 convolutional layers (3 layers of 32 filters with $2 \times 3 \times 3$, and 1 2×2 kernels having strides 1, 1, and 2; then 2 with 64 filters, 1 3×3 then 1 2×2 with strides 1 and 2) followed by one fully connected (200) layer and one output layer, with RELU activations and a dropout of 0.10. Classifier test accuracy was 99.28% for MNIST and 92.99% for FMNIST.

Figures

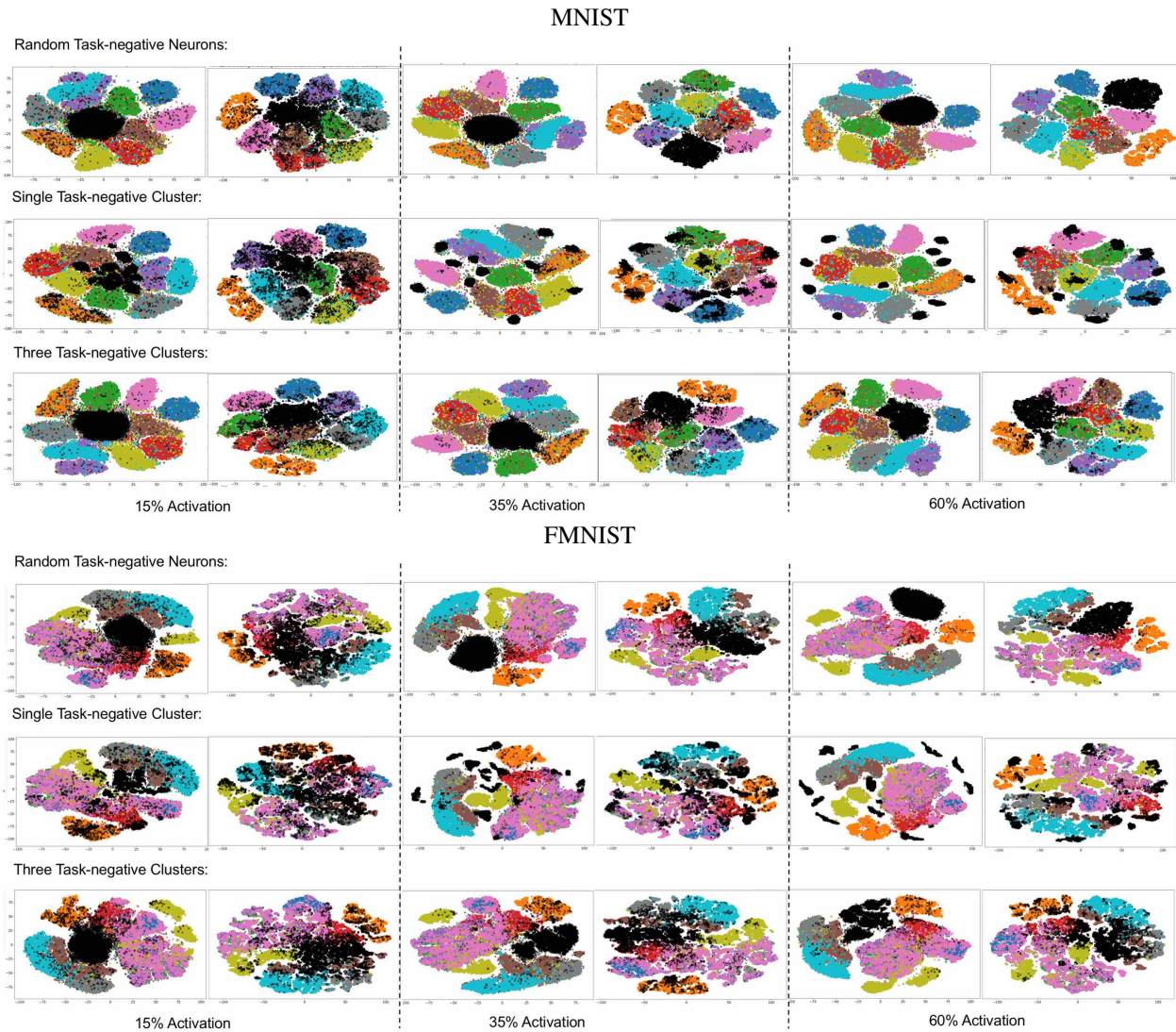


Figure 7: 2D projections, as obtained by performing t-SNE [49] on MNIST (above) and FMNIST (below) ensemble of generated samples and training images. Black dots represent creative samples, while each of the remaining colors denotes a specific MNIST/FMNIST class.

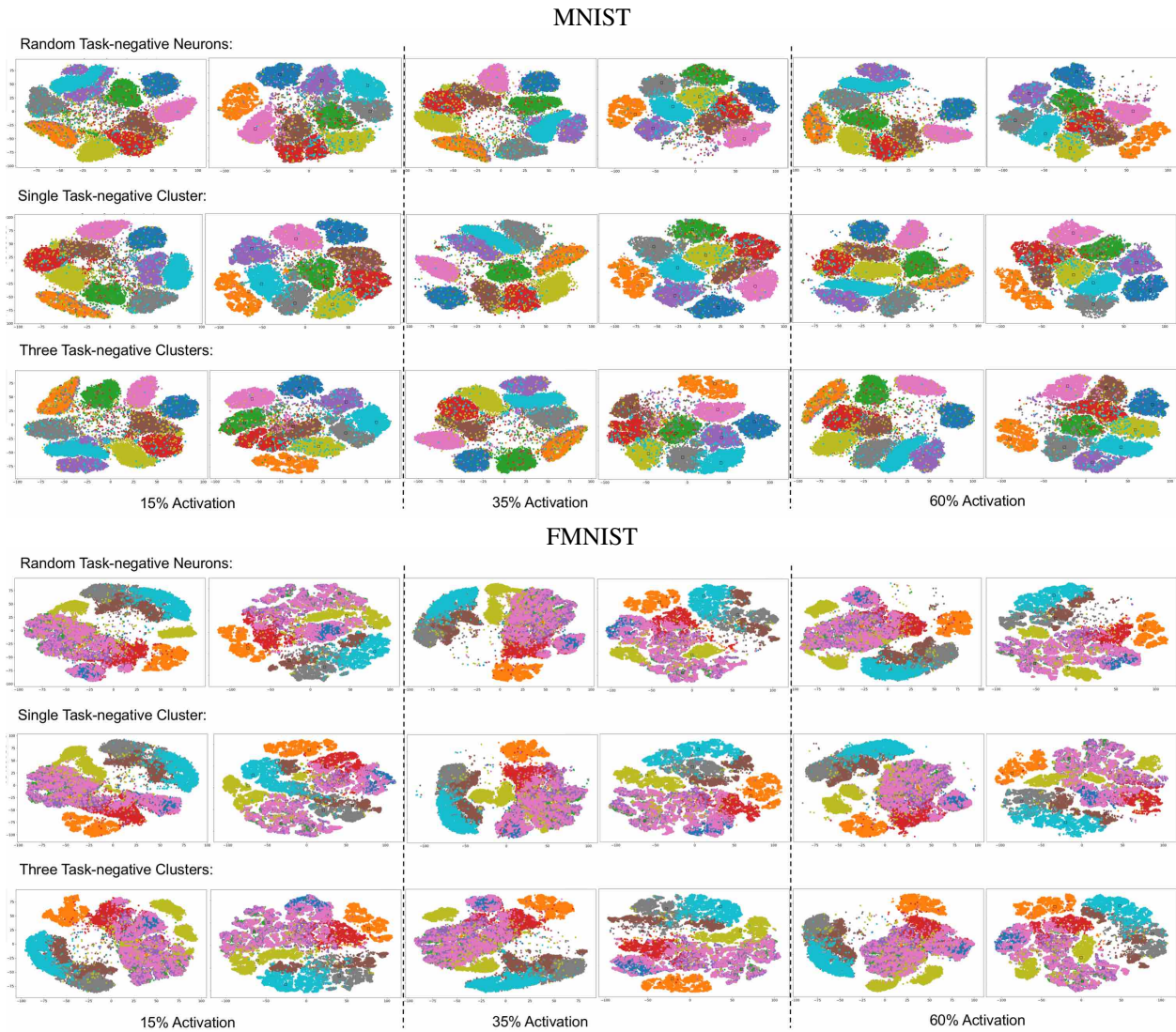


Figure 8: 2D projections, as obtained by performing t-SNE [49] on MNIST (above) and FMNIST (below) ensemble of generated samples and training images, on the input space (left) and on latent space (right). Only training data is shown

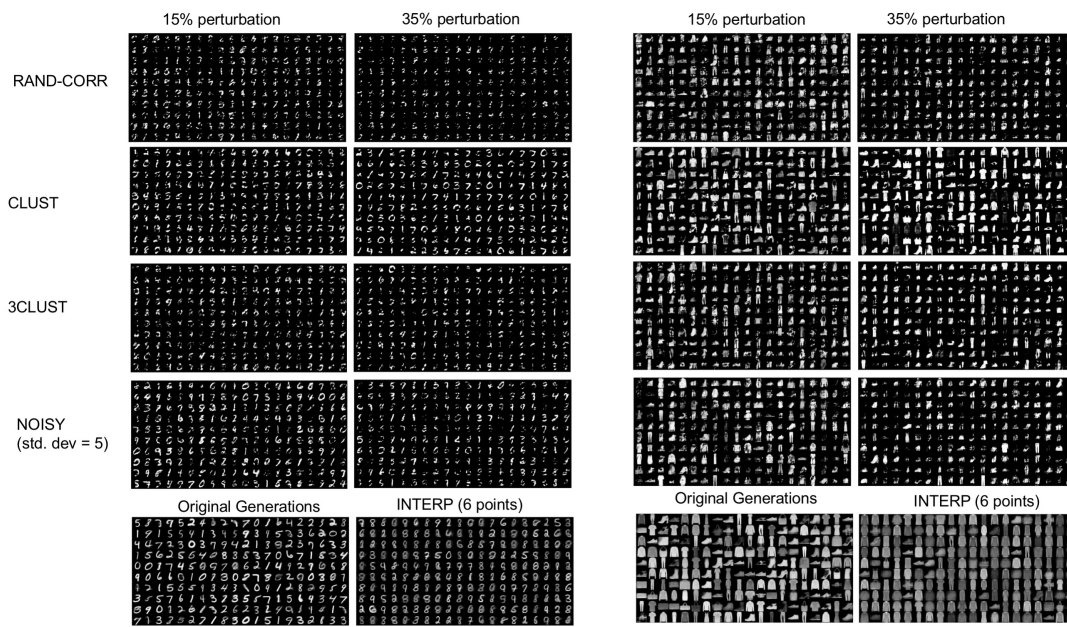


Figure 9: Generated MNIST and FMNIST images.